

International Journal of Modern Physics E  
 © World Scientific Publishing Company

## TOWARDS A UNIFIED DESCRIPTION OF THE ELECTROWEAK NUCLEAR RESPONSE

OMAR BENHAR

*INFN and Department of Physics  
 “Sapienza” University, I-00185 Roma, Italy  
 omar.benhar@roma1.infn.it*

ALESSANDRO LOVATO

*Physics Division, Argonne National Laboratory  
 Argonne, IL 60439, USA  
 lovato@anl.gov*

Received Day Month Year

Revised Day Month Year

We briefly review the growing efforts to set up a unified framework for the description of neutrino interactions with atomic nuclei and nuclear matter, applicable in the broad kinematical region corresponding to neutrino energies ranging between few MeV and few GeV. The emerging picture suggests that the formalism of nuclear many-body theory can be exploited to obtain the neutrino-nucleus cross sections needed for both the interpretation of oscillation signals and simulation of neutrino transport in compact stars.

*Keywords:* neutrino interactions; neutrino-nucleus cross section; neutrino mean free path in nuclear matter.

PACS numbers:24.10.Cn,24.10.Lx,25.30.Pt,26.60.-c

### 1. Introduction

The description of neutrino interactions with nuclei and nuclear matter over a broad kinematical domain, besides being highly valuable in its own right, will be required as an input for the ongoing studies aimed at addressing two outstanding and fundamental physics issues: the violation of CP symmetry in the leptonic sector and the mechanism leading to supernovae explosions.

Interactions of neutrinos of energy ranging from several hundreds MeV to few GeV determine the signals detected by many experimental searches of neutrino oscillations,<sup>1</sup> while the response of uniform nuclear matter to weak interactions at much lower energies, of the order of few MeV, plays a critical role in simulations of neutrino transport in compact stars.<sup>2,3</sup> In the region of high momentum transfer—typically  $|\mathbf{q}| \gtrsim 500$  MeV—in which nuclear interactions can be described within the impulse approximation (IA) scheme,<sup>4</sup> the main difficulties involved in

## 2 Authors' Names

theoretical calculations of the neutrino-nucleus cross section arise from the necessity of combining a realistic model of nuclear structure and dynamics with a proper treatment of relativistic effects, which are known to be large. In the region of low  $|\mathbf{q}|$ , on the other hand, the non relativistic approximation can be safely applied, but the scattering process may involve more than one nucleon, thus leading to the appearance of collective nuclear excitations.

Electron scattering studies have provided ample evidence that in the IA regime the approach based on the factorisation *ansatz* and the spectral function formalism provides a viable computational framework to carry out accurate calculations of the nuclear inclusive cross sections. Of critical importance, in this context, is the use a dynamical model based on a realistic nuclear hamiltonian, allowing to take into account short range nucleon-nucleon (NN) correlations. Recently, the authors of Refs. 5, 6 have shown that, within the approach based on correlated basis function and the cluster expansion technique, the *same* hamiltonian can also be employed to obtain an effective interaction suitable for describing long range correlations—which are known to become important in the low energy regime—in a fully consistent fashion.

The structure of the neutrino-nucleus cross section is outlined in Section 2, while Section 3 is devoted to a brief review of the dynamical model underlying Nuclear Many-Body Theory (NMBT). The formalism employed to describe the kinematical regimes corresponding to low and high energies are discussed in Sections 4 and 5, respectively, while in Section 6 we summarise the main results and state the conclusions.

## 2. The lepton-nucleus cross section

For definiteness, we shall consider charged-current neutrino-nucleus interactions. However, the formalism outlined in this section can be readily generalised to the case of neutral current interactions.<sup>6,7</sup>

The double differential cross section of the process

$$\nu_\ell + A \rightarrow \ell^- + X, \quad (1)$$

where  $A$  and  $X$  denote the target nucleus in its ground state and the undetected nuclear final state, respectively, can be written in the form (see, e.g., Ref. 8)

$$\frac{d^2\sigma}{d\hat{\mathbf{k}}' dk'_0} = \frac{G_F^2 V_{ud}^2}{16\pi^2} \frac{|\mathbf{k}'|}{|\mathbf{k}|} L^{\mu\nu} W_{\mu\nu}. \quad (2)$$

In the above equation,  $k \equiv (k_0, \mathbf{k})$  and  $k' \equiv (k'_0, \mathbf{k}')$  are the four momenta carried by the incoming neutrino and the outgoing charged lepton, respectively,  $\hat{\mathbf{k}}' = \mathbf{k}'/|\mathbf{k}'|$ ,  $G_F$  is the Fermi coupling constant and  $V_{ud}$  is the CKM matrix element coupling  $u$  and  $d$  quarks.

The tensor  $L_{\mu\nu}$  is completely determined by lepton kinematics, whereas the nuclear tensor  $W_A^{\mu\nu}$ , containing all the information on strong interaction dynamics,

describes the response of the target nucleus to weak interactions. Its definition

$$W_{\mu\nu} = \sum_X \langle 0 | J_\mu^\dagger | X \rangle \langle X | J_\nu | 0 \rangle \delta^{(4)}(p_0 + q - p_X), \quad (3)$$

with  $q \equiv (\omega, \mathbf{q}) = k - k'$ , involves the initial and final states  $|0\rangle$  and  $|X\rangle$ , with four momenta  $p_0$  and  $p_X$ , respectively, as well as the nuclear current operator,  $J^\mu$ .

Note that the target ground state  $|0\rangle$  is independent of momentum transfer, while the state  $|X\rangle$  includes at least one particle carrying momentum  $\sim \mathbf{q}$ , and the current operator depends explicitly on  $\mathbf{q}$ . As a consequence, a fully consistent theoretical calculation of the response tensor is only possible in the kinematical regime corresponding to  $|\mathbf{q}|/m \ll 1$ , with  $m$  being the nucleon mass, where the non relativistic approximation underlying NMBT is applicable.<sup>9,10</sup>

On the other hand, the treatment of the region of high momentum transfer, relevant to event analysis of many neutrino experiments, requires a theoretical approach in which the accurate description of the nuclear ground state provided by NMBT is combined with a relativistically consistent description of both the final state and the nuclear current.

### 3. Modelling nuclear structure and dynamics

Nuclear Many-Body Theory (NMBT) is based on the tenet that nucleons can be treated as point like non relativistic particles, the dynamics of which are described by the hamiltonian

$$H = \sum_{i=1}^A \frac{\mathbf{p}_i^2}{2m} + \sum_{j>i=1}^A v_{ij} + \sum_{k>j>i=1}^A V_{ijk}. \quad (4)$$

In the above equation,  $\mathbf{p}_i$  is the momentum of the  $i$ -th nucleon, while the potentials  $v_{ij}$  and  $V_{ijk}$  describe two- and three-nucleon interactions, respectively.

The nucleon-nucleon (NN) potential is obtained from an accurate fit to the available data on the two-nucleon system, in both bound and scattering states, and reduces to the Yukawa one-pion-exchange potential at large distances. State-of-the-art parametrizations of  $v_{ij}$  are written in the form<sup>11</sup>

$$v_{ij} = \sum_{n=1}^{18} v^n(r_{ij}) O_{ij}^n, \quad (5)$$

with  $r_{ij} = |\mathbf{r}_i - \mathbf{r}_j|$  and

$$O_{ij}^{n \leq 6} = [1, (\boldsymbol{\sigma}_i \cdot \boldsymbol{\sigma}_j), S_{ij}] \otimes [1, (\boldsymbol{\tau}_i \cdot \boldsymbol{\tau}_j)], \quad (6)$$

where  $\boldsymbol{\sigma}_i$  and  $\boldsymbol{\tau}_i$  are Pauli matrices acting in spin and isospin space, respectively, and

$$S_{ij} = \frac{3}{r_{ij}^2} (\boldsymbol{\sigma}_i \cdot \mathbf{r}_{ij})(\boldsymbol{\sigma}_j \cdot \mathbf{r}_{ij}) - (\boldsymbol{\sigma}_i \cdot \boldsymbol{\sigma}_j). \quad (7)$$

#### 4 Authors' Names

The operators corresponding to  $n = 7, \dots, 14$  are associated with the non static components of the NN interaction, while those corresponding to  $p = 15, \dots, 18$  account for small violations of charge symmetry. Being fit to the full Nijmegen phase-shift database, as well as to low energy scattering parameters and deuteron properties, the Argonne  $v_{18}$  potential provides an accurate description of the two-nucleon system by construction.

The inclusion of the additional three-body term,  $V_{ijk}$ , is needed to explain the binding energies of the three-nucleon systems.<sup>12</sup> The derivation of  $V_{ijk}$  was first discussed in the pioneering work of Fujita and Miyazawa,<sup>13</sup> who argued that its main contribution originates from the two-pion exchange process in which a NN interaction leads to the excitation of one of the participating particles to a  $\Delta$  resonance, which then decays in the aftermath of the interaction with a third nucleon.

Commonly used models of the three-nucleon potential are written in the form

$$V_{ijk} = V_{ijk}^{2\pi} + V_{ijk}^N, \quad (8)$$

where  $V_{ijk}^{2\pi}$  is the attractive Fujita-Miyazawa term, while  $V_{ijk}^N$  is a purely phenomenological repulsive term. The parameters entering the definition of the above potential are adjusted in such a way as to reproduce the ground state energy of the three-nucleon systems. Note that for  $A=3$  the Schrödinger equation can still be solved exactly, using both deterministic or stochastic methods.

The nuclear current consists of one- and two-nucleon contributions, the latter arising from processes in which the interaction with the beam particle involves a meson exchanged between the target nucleons. It can be conveniently written in the form

$$J^\mu = J_1^\mu + J_2^\mu = \sum_i j_i^\mu + \sum_{j>i} j_{ij}^\mu. \quad (9)$$

The connection between the above current operator and the nuclear hamiltonian will be discussed in the next section.

#### 4. Nonrelativistic regime

In the nonrelativistic regime, typically corresponding to  $|\mathbf{q}| \lesssim 500$  MeV, both the initial and the final state appearing in Eq. (3) are eigenstates of the nonrelativistic many-body hamiltonian of Eq. (4), satisfying the Schrödinger equations

$$H|0\rangle = E_0|0\rangle, \quad H|X\rangle = E_X|X\rangle. \quad (10)$$

In the case of light nuclear targets, the ground state wave function can be obtained from accurate stochastic approaches, such as Green's Function Monte Carlo (GFMC).<sup>14,15</sup> In addition, the nuclear cross section can be conveniently rewritten in terms of the response functions  $R_{\mu\nu}(q, \omega)$ , obtained from Eq.(3) replacing the components of the current operator with their expressions obtained in the relativistic limit, taking into account terms up to order  $(|\mathbf{q}|/m)^2$ .

A fundamental feature of the description of neutrino-nucleus interactions at low and moderate momentum transfer is the possibility of employing a set of electroweak charge and current operators consistent with the hamiltonian of Eq.(4).

The nuclear electromagnetic current,  $J_{\text{em}}^\mu \equiv (J_{\text{em}}^0, \mathbf{J}_{\text{em}})$ , trivially related to the vector component of the weak current, is constrained by  $H$  through the continuity equation<sup>16</sup>

$$\nabla \cdot \mathbf{J}_{\text{em}} + i[H, J_{\text{em}}^0] = 0 . \quad (11)$$

Note that, because the NN potential  $v_{ij}$  does not commute with the charge operator  $J_{\text{em}}^0$ , the above equation implies that  $J_{\text{em}}^\mu$  involves two-nucleon contributions, as shown in Eq.(9).

The one-body electroweak operator is obtained from a non relativistic expansion of the covariant single-nucleon currents. Two-body charge and current operators are derived within the conventional meson-exchange formalism<sup>17,18</sup> or within the Effective Field Theory approach inspired to chiral perturbation theory ( $\chi$ EFT).<sup>19-23</sup> In this short review we will mainly discuss the former, in which the dominant static part of the realistic two-nucleon potential arises from exchange of effective pseudoscalar ( $\pi$ -like) and vector ( $\rho$ -like) mesons, and the corresponding charge and current operators are projected out of the static components of the potential. As a consequence, the resulting vector current is conserved by construction.

The conventional electroweak charge and current operators have no free parameters, except the nucleon-to- $\Delta$  axial coupling constant, which is fixed by reproducing the tritium Gamow-Teller transition strength in calculations based on the realistic hamiltonian discussed above.

Nonrelativistic meson-exchange currents (MEC) have been used in analyses of a variety of electromagnetic moments and electroweak transitions of s- and p-shell nuclei at low and intermediate values of energy and momentum transfers. Taking MEC into account, a good agreement has been achieved between theoretical predictions and experimental data for the  $M1$  and  $E2$  radiative transition rates between low-lying states,<sup>24,25</sup>  $\beta$ -decays and electron- and muon-capture rates,<sup>26,27</sup> elastic and inelastic form factors measured in  $(e, e')$  scattering<sup>10,28-30</sup> and radiative and weak capture reactions at low energies.<sup>17</sup>

#### 4.1. Quantum Monte Carlo approach

Quantum Monte Carlo (QMC) methods were first applied to the study of properties of light nuclei over three decades ago<sup>31</sup> (for a recent review of Quantum Monte Carlo methods for nuclear physics see, e.g., Ref. 32). Within the limits of applicability of NMBT, they provide a truly *ab initio* approach, allowing to perform exact calculations of a number of nuclear properties.

6 *Authors' Names*

 4.1.1. *QMC calculations of the nuclear ground state*

The first calculations employed the variational Monte Carlo (VMC) technique, in which the stochastic Metropolis algorithm is used for evaluating the expectation value of a given many-body operator using a suitably parametrized trial wave function,  $\Psi_T$ . The parameters entering the definition of  $\Psi_T$  are optimized by minimizing the variational energy

$$E_V = \frac{\langle \Psi_T | H | \Psi_T \rangle}{\langle \Psi_T | \Psi_T \rangle} \geq E_0 , \quad (12)$$

which provides an upper bound to the ground-state energy  $E_0$ . It is worth noting that Monte Carlo methods can also be used in the search for the best variational parameters.

Designing an accurate variational wave function requires a deep understanding of both the structure and dynamics of the nuclear system under consideration. Standard VMC calculations for light nuclei use a variational wave function of the form

$$|\Psi_T\rangle = \mathcal{F}|\Phi\rangle . \quad (13)$$

The long-range behaviour is described by the Slater determinant  $|\Phi\rangle$ . For example, in the case of uniform nucleon matter in the normal (i.e. non superfluid) phase,  $|\Phi\rangle$  is the wave function describing a non interacting Fermi gas. For light nuclei, on the other hand,  $|\Phi\rangle$  is usually written as a sum of Slater determinants, such as those resulting from a small scale shell-model calculation.

The short-range components of the wave functions are controlled by the correlation operator  $\mathcal{F}$ , the structure of which reflects the complexity of the two- and three-nucleon potentials appearing in the nuclear hamiltonian

$$\mathcal{F} \equiv \left( \mathcal{S} \prod_{i < j < k} F_{ijk} \right) \left( \mathcal{S} \prod_{i < j} F_{ij} \right) . \quad (14)$$

In the above equation,  $\mathcal{S}$  is the symmetrisation operator, needed to fulfill the requirement of antisymmetrisation of the trial wave function, while the two-body correlation operator exhibits a spin-isospin structure similar to that of the NN potential [compare to Eq.(5)]

$$F_{ij} = \sum_n f^n(r_{ij}) O_{ij}^n , \quad (15)$$

implying that  $[F_{ij}, F_{ik}] \neq 0$ . The scalar,  $f^c = f^1$ , and operator,  $f^{n>1}$ , pair correlation functions reflect the influence of the the short-distance behavior of the two-body potential and, at the same time, satisfy the boundary conditions implied by the requirement of cluster separability.

As discussed below (see Section 4.2), reasonably accurate correlation functions are generated by minimising the two-body cluster contribution to the energy per particle. This procedure results in the derivation of eight Euler-Lagrange differential equations, involving a set of variational parameters.<sup>33</sup>

Three-body correlation functions are induced by both the two- and three-body potentials. As for the latter case, the form suggested by perturbation theory

$$F_{ijk} = 1 + \sum_x \epsilon_x V_{ijk}(y r_{ij}, y r_{jk}, y r_{ik}), \quad (16)$$

is usually employed. In the above equation, the subscript  $x$  labels the various contributions to the three-body force, the  $\epsilon_x$  are small negative strength parameters, and  $y$  is a scaling factor.

The GFMC method<sup>14,15</sup> overcomes the limitations of the variational wavefunction by using an imaginary-time projection technique to enhance the ground-state component of the starting trial wave function. The method relies on the observation that  $\Psi_T$  can be expanded in the complete set of eigenstates of the the hamiltonian according to

$$|\Psi_T\rangle = \sum_n c_n |n\rangle \quad , \quad H|n\rangle = E_n |n\rangle \quad , \quad (17)$$

which implies

$$\lim_{\tau \rightarrow \infty} e^{-(H-E_0)\tau} |\Psi_T\rangle = c_0 |0\rangle \quad , \quad (18)$$

where  $\tau$  is the imaginary time. Hence, GFMC projects out the exact lowest-energy state, provided  $\Psi_T$  it is not orthogonal to the true ground state, i.e.  $c_0 \neq 0$ .

The direct calculation of  $\exp[-(H-E_0)\tau]$  for strongly-interacting systems involves prohibitive difficulties. To circumvent this problem, the imaginary-time evolution is broken into  $N$  small imaginary-time steps, and complete sets of states are inserted, in such a way that only the calculation of the short-time propagator is required. This procedure yields the expression

$$\begin{aligned} \langle \mathbf{R}_{N+1} | e^{-(H-E_0)\tau} | \mathbf{R}_1 \rangle &= \int \langle \mathbf{R}_{N+1} | e^{-(H-E_0)\Delta\tau} | \mathbf{R}_N \rangle \langle \mathbf{R}_N | e^{-(H-E_0)\Delta\tau} | \mathbf{R}_{N-1} \rangle \dots \\ &\times \langle \mathbf{R}_2 | e^{-(H-E_0)\Delta\tau} | \mathbf{R}_1 \rangle dR_2 \dots dR_N \quad , \end{aligned} \quad (19)$$

where, for the sake of simplicity, the dependence on the spin-isospin degrees of freedom have been omitted.

Monte Carlo techniques are used to sample the paths  $\mathbf{R}_i$  in the propagation. Note that, while being exact only in the  $\Delta\tau \rightarrow 0$  limit, the accuracy of Eq.(19) can be checked by performing several simulations with smaller time step and extrapolating to zero.

Because nuclear interactions are strongly spin-isospin dependent, the trial wave function is written as a a sum of complex amplitudes for each spin-isospin state of the system

$$|\Psi_T\rangle = \sum_{s,t} \psi_T(\mathbf{R}) |\chi_s(\sigma)\rangle |\chi_t(\tau)\rangle \quad . \quad (20)$$

Within standard GFMC for nuclear physics applications,<sup>34,35</sup> the  $2^A$  many-body spin states, defined as

$$\begin{aligned}
 \chi_{s=1} &= |\downarrow_1, \downarrow_2, \dots, \downarrow_A\rangle \\
 \chi_{s=2} &= |\uparrow_1, \downarrow_2, \dots, \downarrow_A\rangle \\
 &\dots \\
 \chi_{s=2^A} &= |\uparrow_1, \uparrow_2, \dots, \uparrow_A\rangle
 \end{aligned} \tag{21}$$

are considered. The corresponding many-body isospin states can be obtained by replacing  $\uparrow$  and  $\downarrow$  with  $p$  and  $n$ . Exploiting charge conservation, the  $2^A$  isospin states can be reduced to  $A!/(N!Z!)$  states and, by assuming that the total isospin  $T$  is a good quantum number for the nucleus, the size of  $|\chi_t(\tau)\rangle$  can be further decreased.

Because the GFMC imaginary-time evolution of Eq. (19) involves a sum over spin and isospin states at each step, the computing time grows exponentially with the number of particles. The largest calculations to date have been performed for the nucleus of  $^{12}\text{C}$  and for the systems of 16 neutrons, corresponding to 540,672 and 65,536 spin-isospin states, respectively.

Over the past decade, the Auxiliary Field Diffusion Monte Carlo (AFDMC) has emerged as a more efficient algorithm for dealing with larger nuclear system.<sup>36</sup> Within AFDMC, the spin-isospin degrees of freedom are described by single-particle spinors, the amplitudes of which are sampled using Monte Carlo techniques, and the coordinate-space diffusion in GFMC is extended to include diffusion in spin and isospin spaces.

The early applications of AFDMC were based on variational wave function containing purely central correlation functions, and the accuracy of this approach for systems other than pure neutron matter was limited. Recently, the authors of Ref. 37 were able to add operator correlations to the trial wave function, and developed a novel importance sampling technique, making the accuracy of AFDMC comparable to that of GFMC even in systems containing both protons and neutrons.

#### 4.1.2. *QMC studies of the response functions*

The calculation of the response functions involves major difficulties even in the region of  $|\mathbf{q}| \lesssim 0.5$  GeV and  $\omega$  corresponding to quasi-free kinematics, where the consequences of the nucleon's internal structure on nuclear dynamics can be subsumed into effective many-body potentials and currents.

Integral properties of the response functions can be studied exploiting their sum rules, which are obtained from ground-state expectation values of appropriate combinations of the current operators, thus avoiding the calculation of the full excitation spectrum of the target nucleus. GFMC calculations of the electromagnetic

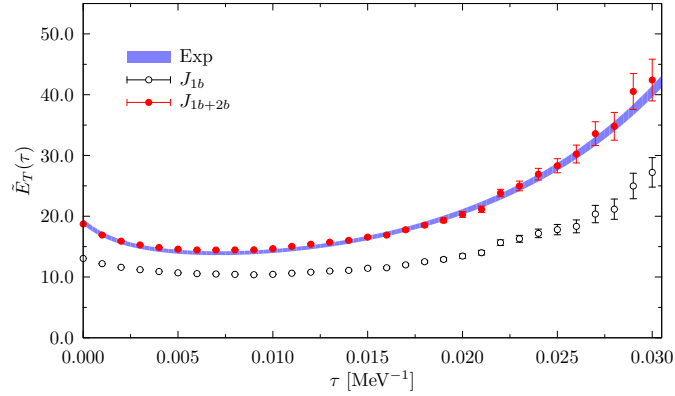


Fig. 1. Euclidean electromagnetic response function of  $^{12}\text{C}$  in the transverse channel at  $|\mathbf{q}| = 570$  MeV. Experimental data are taken from Ref. 38.

sum rules,<sup>39</sup> have demonstrated that a large fraction ( $\simeq 30\%$ ) of the strength in the transverse channel arises from processes involving two-body currents, and that interference effects between the matrix elements of one- and two-body currents play a major role.<sup>40</sup> These effects are typically only partially, or approximately, accounted for in existing perturbative or mean-field studies.<sup>41–44</sup>

The main drawback of the sum rules is that they do not provide any information on the distribution of strength; whether, for example, the calculated excess strength induced by two-body currents is mostly at large  $\omega$ , well beyond the quasi-elastic peak, or it is also found in the quasi-elastic region. In addition, in the electromagnetic case, comparison of theoretical and experimental sum rules is problematic, since longitudinal and transverse response functions obtained from Rosenbluth separation of the measured inclusive ( $e, e'$ ) cross sections are only available in the space-like region ( $\omega < |\mathbf{q}|$ ) and therefore must be extrapolated into the unobserved time-like region ( $\omega > |\mathbf{q}|$ ) before “experimental” values for the sum rules can be determined.<sup>39</sup>

Valuable information on the  $\omega$  dependence of the response functions can be inferred from their Laplace transforms, also referred to as Euclidean responses,<sup>45</sup> defined as

$$E_{\mu\nu}(q, \tau) = C_{\mu\nu}(q) \int_{\omega_{\text{th}}}^{\infty} d\omega e^{-\tau\omega} R_{\mu\nu}(q, \omega), \quad (22)$$

where  $\omega_{\text{th}}$  is the inelastic threshold and the  $C_{\mu\nu}$  are  $q$ -dependent normalization factors. In the case of the electromagnetic longitudinal ( $L$ , or  $\mu\nu = 00$ ) and transverse ( $T$ , or  $\mu\nu = xx$ ) response functions, the normalization factors are<sup>45</sup>  $C_L = C_T = 1/[G_E^p(Q_{\text{qe}}^2)]^2$ , where  $G_E^p$  is the proton electric form factor and

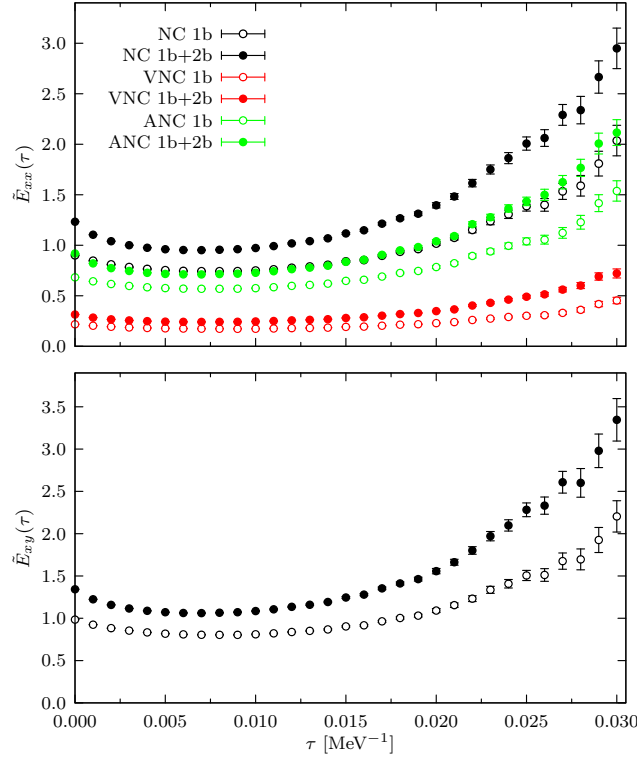


Fig. 2. Euclidean neutral-weak  $E_{xx}$  (top panel) and  $E_{xy}$  (lower panel) response functions of  $^{12}\text{C}$  at  $|\mathbf{q}| = 570$  MeV.

$Q_{\text{qe}}^2 = |\mathbf{q}|^2 - \omega_{\text{qe}}^2$ ,  $\omega_{\text{qe}}$  being the energy transfer corresponding to quasi free kinematics. In the neutral-weak response functions the normalisation factors are the same as those adopted in calculations of the sum rules.<sup>46</sup>

The chief advantage of the Euclidean response is that it can be expressed as a ground-state expectation value

$$\frac{E_{\mu\nu}(|\mathbf{q}|, \tau)}{C_{\mu\nu}} = \frac{\langle 0 | O_{\alpha}^{\dagger}(\mathbf{q}) e^{-(H-E_0)\tau} O_{\beta}(\mathbf{q}) | 0 \rangle}{\langle 0 | e^{-(H-E_0)\tau} | 0 \rangle}, \quad (23)$$

where  $H$  is the nuclear Hamiltonian, and  $E_0$  is a trial energy controlling the normalisation.

In Fig. 1, taken from Ref. 47, the electromagnetic transverse Euclidean response function of  $^{12}\text{C}$ ,  $E_T$ , is compared to the one obtained from the analysis of the world data carried out by Jourdan,<sup>38</sup> represented by the shaded band. The procedure followed to obtain the *experimental* Euclidean response is discussed in Ref. 47. Note that, in order to emphasise the large  $\tau$  behavior, the scaled Euclidean response  $\tilde{E}_{\mu\nu}(|\mathbf{q}|, \tau) = \exp[\tau \mathbf{q}^2 / (2m)] E_{\mu\nu}(|\mathbf{q}|, \tau)$  is displayed. The results obtained by including only one-body or both one- and two-body terms in the electromagnetic

transition operators are represented by open and solid circles, respectively. Two-body current contributions substantially increase the Euclidean response over the whole range of imaginary-time, thus implying that excess transverse strength is generated by two-body currents not only at  $\omega \gtrsim \omega_{qe}$ , but also in the quasi-elastic and threshold regions. The full predictions obtained including two-body currents are in excellent agreement with data.

A similar enhancement brought about by the two-body currents has been observed in the Euclidean neutral-weak response functions,<sup>47</sup> displayed in Fig. 2. The neutral-current response  $E_{xy}(|\mathbf{q}|, \tau)$  is due to the interference between the vector (VNC) and axial-vector (ANC) terms of the neutral current (NC), and in the inclusive cross section the corresponding  $R_{xy}(|\mathbf{q}|, \omega)$  enters with opposite sign depending on whether the process  $A(\nu_l, \nu'_l)$  or  $A(\bar{\nu}_l, \bar{\nu}'_l)$  is considered.<sup>48</sup> Hence, the difference between the neutrino and antineutrino cross sections turns out to be proportional to  $R_{xy}$ . This difference may well have an impact on the determination of the CP-violating phase from neutrino and antineutrino events detected at DUNE.<sup>49</sup>

On the other hand, since for  $E_{xx}(|\mathbf{q}|, \tau)$  the interference between vector and axial-vector terms vanishes, the response is simply given by the sum of the terms with both transition operators arising from either the VNC or the ANC. For  $E_{xx}(|\mathbf{q}|, \tau)$  these individual contributions, along with their sum, are displayed separately. Both the  $E_{xx}(|\mathbf{q}|, \tau)$  and  $E_{xy}(|\mathbf{q}|, \tau)$  response functions obtained retaining one-body terms only in the NC are substantially increased when two-body terms are also included. This enhancement is found not only at low  $\tau$ , thus corroborating the sum-rule predictions of Ref. 46, but in fact extends over the whole  $\tau$  region. Moreover, the individual (VNC-VNC) and (ANC-ANC) contributions are about equally affected.

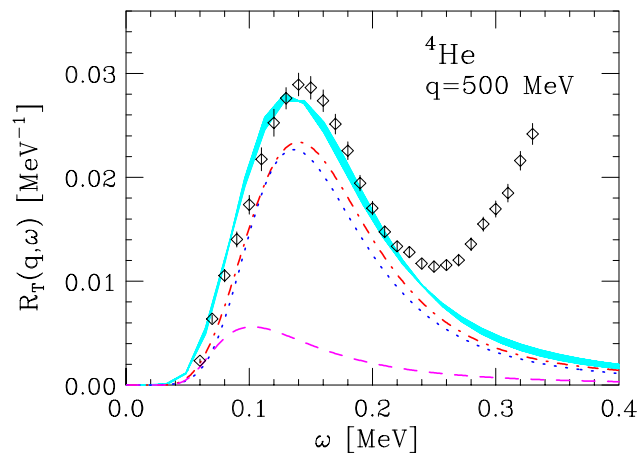


Fig. 3. (Color online) Transverse electromagnetic response functions of  ${}^4\text{He}$  at  $|\mathbf{q}| = 500$  MeV. Experimental data are from Ref. 45.

The inversion of the Laplace transform, needed to retrieve the energy dependence of the responses, is long known to involve severe difficulties. A groundbreaking result has been recently reported by the authors of Ref. 47, who exploited the maximum entropy technique to obtain the electromagnetic longitudinal and transverse responses of  ${}^4\text{He}$ .

Figure 3 shows the breakdown of the transverse response of  ${}^4\text{He}$  at  $|\mathbf{q}| = 500$  MeV into one-nucleon current, two-nucleon current and interference contributions.<sup>50</sup> Note that the quantity displayed in the figure is normalized dividing by the squared proton form factor. It clearly appears that including the two-nucleon currents leads to a sizable enhancement of the response, and that the large positive contribution of the interference term peaks at energy loss  $\omega < \omega_{qe}$ . The agreement between the GFMC results and the data of turns out to be remarkably good.

#### 4.2. *Correlated Basis Functions and Cluster Expansion Formalism*

The Green's Function Monte Carlo method, while providing a most powerful computational scheme to carry out *exact* calculations of a variety of nuclear properties and scattering observables, is still limited to light nuclei, with  $A \leq 12$ . An alternative approach, which has been extensively employed to study both medium-heavy nuclei<sup>51</sup> and nuclear matter,<sup>52</sup> is based on the use of correlated basis functions (CBF) and the cluster expansion technique (see, e.g., Refs. 53, 54, 55).

Let us consider, for simplicity, uniform and isospin symmetric nuclear matter. In the is case, the correlated states are obtained from the corresponding states of the non interacting Fermi gas,  $|N\rangle_{\text{FG}}$ , through the transformation

$$|N\rangle = \frac{F|N\rangle_{\text{FG}}}{\text{FG}\langle N|F^\dagger F|N\rangle_{\text{FG}}^{1/2}}. \quad (24)$$

The operator  $F$ , embodying the correlation structure induced by the NN interaction, is written in the form (compare to Eq.(15))

$$F = \mathcal{S} \prod_{ij} F_{ij}. \quad (25)$$

The two-body correlation functions  $F_{ij}$ , whose operator structure reflects the complexity of the NN potential, is written in the form

$$f_{ij} = \sum_{n=1}^6 f^n(r_{ij}) O_{ij}^n, \quad (26)$$

including the contributions associated with the operators  $O_{ij}^{n \leq 6}$  of Eq.(6).

The explicit calculation of matrix elements of a many-body operator, such as the nuclear hamiltonian  $H$ , between correlated states involves prohibitive difficulties, because it requires integrations over the coordinates—as well as summations over the discrete degrees of freedom—of many nucleons. This problem can be circumvented expanding the matrix elements in series, the terms of which represent

the contributions of subsystems (clusters) containing an increasing number (2, 3, ..., A) of particles.

Within the cluster expansion approach, the expectation value of the hamiltonian in the correlated nuclear matter ground state, the minimum of which provides the variational estimate of the corresponding energy, can be written as<sup>54</sup>

$$E_V = \langle 0|H|0 \rangle = T_0 + \sum_n (\Delta E_V)_n , \quad (27)$$

where the first term in the right hand side is the energy of the non interacting Fermi gas. The contributions to the cluster expansion (27) can be represented by diagrams and classified according to their topological structures. Selected classes of diagrams can then be summed to all orders, solving a set of integral equations referred to as Fermi Hyper-Netted Chain (FHNC) equations,<sup>54</sup> to obtain an accurate estimate of  $E_V$

The correlation functions  $f^n(r_{ij})$  are determined from the minimisation of the expectation value of the Hamiltonian. The functional minimisation of the two-body cluster contribution to the energy per particle,  $(\Delta E_V)_2$ , leads to a set of six Euler-Lagrange equations, to be solved with proper constraints that force  $f^c$  and  $f^{(n>1)}$  to “heal” to one and zero, respectively. This is most efficiently achieved through the boundary conditions<sup>56</sup>

$$f^n(r \geq d_n) = \delta_{n1} \quad , \quad \left. \frac{df^n(r)}{dr} \right|_{d_n} = 0 , \quad (28)$$

where the healing distances  $d_n$  are treated as variational parameters, to be determined from the minimisation of  $E_V$ . Additional variational parameters are the quenching factors  $\alpha_n$  which simulate modifications of the nucleon-nucleon potential, arising from the screening induced by the presence of the nuclear medium, and the set of scaling factors  $\beta_n$ , often applied to the correlation functions  $f^n$ .

### 4.3. The CBF effective interaction

The applications of the formalism of correlated basis function to the study of the nuclear matter response at low momentum transfer exploit the CBF effective interaction

$$V^{\text{eff}} = \sum_{j>i} v_{ij}^{\text{eff}} , \quad (29)$$

defined by the relation<sup>57</sup>

$$\langle H \rangle = \langle 0|H|0 \rangle = T_0 + {}_{\text{FG}} \langle 0|V_{\text{eff}}|0 \rangle_{\text{FG}} . \quad (30)$$

The left hand side of the above equation, computed within the variational approach using the FHNC summation scheme, is assumed to provide a good approximation to the ground state energy, while the right hand side is computed at low order of the cluster expansion, i.e. two- or three-body cluster level. The range of the correlations

is adjusted in such a way as to satisfy Eq. (30), which implies that the low order calculation reproduces the variational ground state energy.

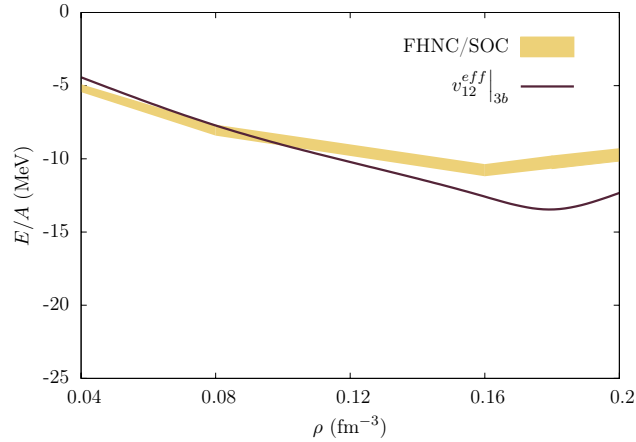


Fig. 4. Density dependence of the energy per particle of isospin symmetric nuclear matter in the low density regime, computed with a bare hamiltonian containing the Argonne  $v_6'$  potential and the UIX three-body interaction model. The solid line displays the results obtained using the CBF effective interaction, while the full variational energy per particle is represented by the shaded region, accounting for the uncertainty arising from the treatment of the kinetic energy term.<sup>5</sup>

The authors of Ref. 57, who performed the first calculation of  $V^{\text{eff}}$  of Eq.(30), took into account two-body cluster diagrams only. This prescription, while leading to a very simple and transparent expression of  $V^{\text{eff}}$ , fails to account for three-body forces, which are long known to play a critical role in determining the energy spectrum of light nuclei, as well as the saturation properties of isospin symmetric nuclear matter.

The approach proposed in Ref. 58, in which interactions involving more than two nucleons are included through a density dependent modification of the NN potential at intermediate range, has been implemented in the effective interaction formalism in Refs. 59, 60. More recently, the CBF effective interaction has been substantially improved by the authors of Refs. 5, 6, who explicitly included the three-body cluster contributions, allowing for a more realistic description of three-nucleon forces at microscopic level. The energy-dependence of the binding energy per nucleon in isospin symmetric matter obtained from the effective interaction of Refs. 5, 6, which includes the effects of the UIX model of the three-nucleon potential, is illustrated in Fig. 4 (taken from Ref. 5). It turns out to be fairly close to that resulting from the full FHNC calculation, and exhibits saturation, albeit at

density larger than the empirical value  $\rho_0 = 0.16 \text{ fm}^{-3}$ .

#### 4.4. Weak response of nuclear matter at low momentum transfer

The cooling of neutron stars is driven by the energy loss caused by the flux of neutrinos leaving the star. This effect can be conveniently parametrized in terms of the neutrino mean free path (NMFP), which is one of the critical inputs required for large-scale simulations of neutrino transport.<sup>61</sup>

Neutrino and antineutrino interactions in neutron matter are also relevant for understanding the evolution of the very neutron-rich matter formed in neutron-star mergers, since they can potentially affect the neutron to proton ratio and significantly impact the r-process in neutron star mergers, currently considered to be an important source for r-process nucleosynthesis.

The relatively low momentum scale of the above processes, typically  $|\mathbf{q}| \lesssim 50 \text{ MeV}$ , allows for a nonrelativistic treatment of both the current operators and the final states entering the hadronic tensor. Earlier calculations have accounted for the effects of correlations in the nuclear wave function through empirical effective interactions or Landau parameters, derived from Skyrme-like effective interactions, and using the Random Phase Approximation (RPA).<sup>62,63</sup> However, the effect of correlations on the current operators was totally neglected, as bare weak operator were considered. It is well established that such approach is inconsistent, and that a consistent set of effective operators and effective interactions must be included in a more accurate treatment of the nuclear response functions.

The CBF effective interaction approach is best suited to define effective weak-current operators that are consistent with the effective interaction of Eq. (30). Under the assumption that the nonrelativistic final states entering the hadronic tensor can be described by CBF states of Eq. (24), the effective operators can be defined through their transition matrix elements

$$\langle X | J_\mu^{\text{eff}} | 0 \rangle = \frac{{}_{\text{FG}}\langle X | \mathcal{F}^\dagger J_\mu \mathcal{F} | 0 \rangle_{\text{FG}}}{\sqrt{{}_{\text{FG}}\langle 0 | \mathcal{F}^\dagger \mathcal{F} | 0 \rangle_{\text{FG}} {}_{\text{FG}}\langle X | \mathcal{F}^\dagger \mathcal{F} | X \rangle_{\text{FG}}}} = {}_{\text{FG}}\langle X | J_\mu^{\text{eff}} | 0 \rangle_{\text{FG}}. \quad (31)$$

Existing calculations based on the CBF effective interaction approach have only accounted for transitions between the correlated ground-state and correlated one particle-one hole (1p1h) excited states, which amounts to setting  ${}_{\text{FG}}\langle X | J_\mu^{\text{eff}} | 0 \rangle_{\text{FG}} \simeq {}_{\text{FG}}\langle ph | J_\mu^{\text{eff}} | 0 \rangle_{\text{FG}}$ , where  $p$  and  $h$  denote both the momentum and the spin and isospin projections specifying single nucleon state.

The effective operators encompass short-range correlations, but fail to account for long range correlations, responsible for collective modes. The  $|ph\rangle_{\text{FG}}$  states are not eigenstates of the effective hamiltonian and, as a consequence, there is a residual interaction that can induce transitions between different 1p1h states.

The effect of long-range correlations can be included in the effective interaction formalism using the Tamm-Dancoff (TD) approximation, i.e. expanding the final

state in the basis of one 1p1h states according to

$$|X\rangle_{\text{TD}} = \sum_{ph} c_{ph}^X |ph\rangle_{\text{FG}}. \quad (32)$$

The excitation energy  $E_X$  of the state  $|X\rangle$ , as well as the coefficients  $c_{ph}^X$ , are determined by solving the eigenvalue equation

$$H_{\text{eff}}|X\rangle_{\text{TD}} = E_X|X\rangle_{\text{TD}}, \quad (33)$$

with

$$H^{\text{eff}} = -\sum_i \frac{\nabla_i^2}{2m} + \sum_{j>i} v_{ij}^{\text{eff}}. \quad (34)$$

Note that the correlations defining the effective interaction used in the previous equations are the same appearing in the definitions of the effective current operators.

The effect of long-range correlation is apparent in the spin-response of pure neutron matter,<sup>6</sup> displayed in Fig. 5, (taken from Ref. 6). The dashed and dot-dash lines represent the spin-transverse ( $\mu\nu = xx + yy$ ) and spin-longitudinal ( $\mu\nu = zz$ ) response functions of pure neutron matter at density  $\rho = 0.16 \text{ fm}^{-3}$  computed in correlated Tamm-Dancoff (CTD) approximation, respectively. For comparison, the solid line corresponds to the spin-density response obtained from the Landau theory, the parameters of which have been consistently derived from the same effective interaction.<sup>64</sup>

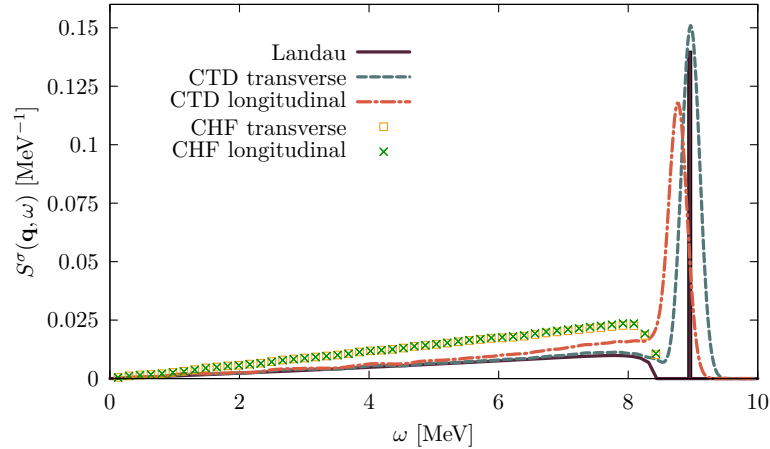


Fig. 5. Spin-transverse (dashed line) and spin-longitudinal (dot-dash line) responses of pure neutron matter, computed within the CTD and CHF approximations at  $\rho = 0.16 \text{ fm}^{-3}$  for momentum transfer  $|\mathbf{q}| = 0.1 \text{ fm}^{-1}$ . The solid line has been obtained from Landau theory, according to the approach of Ref. 64.

When long-range correlations are accounted for, the peak associated with the collective excitation sticks out in both the spin-longitudinal and spin-transverse

channels. On the other hand, in the correlated Hartree-Fock (CHF) scheme, in which nuclear correlations only enter via the effective operators and the quasiparticle energies, the strength of the response function is smoothly distributed over the particle-hole continuum.

Long-range correlations have been shown to produce a similar effect in the Fermi and Gamow-Teller responses of isospin-symmetric nuclear matter,<sup>5,57,60</sup> whereas no collective mode is observed in the neutron matter density response function.<sup>6</sup>

The neutrino mean free path for low energy neutrino scattering and neutrino absorption processes in cold isospin symmetric matter has been found to be largely affected by both short- and long-range correlations.<sup>57</sup> For densities ranging from  $\rho_0/2$  to  $3/2\rho_0$ , the NMFP obtained from the CTD response functions is  $\sim 2.5 - 3.5$  times larger than the one of the noninteracting Fermi Gas case. In addition, the NMFP for scattering is 2 times larger than that for absorption, indicating that the cross section for charged-current transitions is 2 times larger than the one associated with neutral-current process.

The role of long-range correlations in determining the NMFP associated with neutrino scattering processes in cold neutron matter has been investigated within Landau theory in Ref. 64. Figure 6, taken from Ref. 65 shows the density dependence of the mean free path of a non degenerate neutrino with an energy  $E = 1$  MeV. The results of Landau theory, obtained including tensor interaction terms (solid line) and neglecting them (open circles), are compared with those corresponding to a free neutron gas (dot-dashed line). It clearly appears that inclusion of interaction effects leads to a large enhancement of the NMFP over the whole density range. The collective mode of the spin-density response function increases the scattering cross section, hence reducing the NMFP, by about 25%. It is worth nothing that the the results of Fig. 6 have been confirmed by the CTD calculations reported in Ref. 6.

## 5. Relativistic regime

The dynamical model discussed in Section 3 and the formalism of correlated basis functions can be also employed to describe the nuclear response in the kinematical region of large momentum transfer, in which  $|\mathbf{q}|^{-1} \ll d$ , with  $d$  being the average NN separation distance in the target. In this regime nuclear scattering can be reasonably assumed to reduce to the incoherent sum of elementary scattering processes involving individual nucleons, and the IA is expected to be applicable.

Within the IA scenario, the difficulties associated with the relativistic treatment of the nuclear final state and current operator are circumvented exploiting the factorisation *ansatz*, which amounts to: (i) neglecting the contribution of the two-nucleon current, and (ii) rewriting the nuclear final state in the form

$$|X\rangle = |\mathbf{p}\rangle \otimes |n_{A-1}, \mathbf{p}_n\rangle . \quad (35)$$

In the above equation, the state  $|\mathbf{p}\rangle$  describes a non interacting nucleon, while

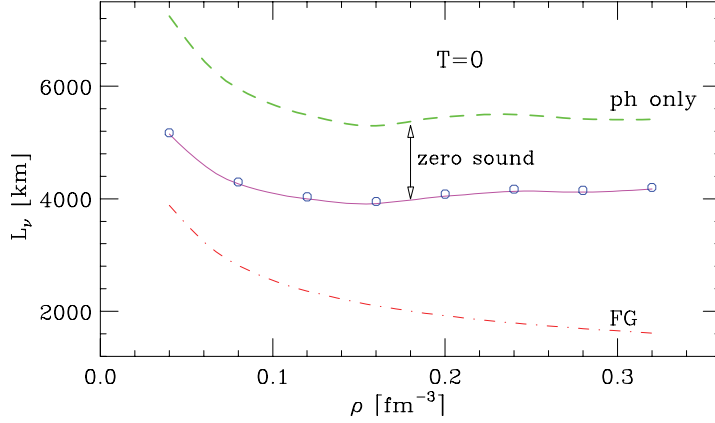


Fig. 6. Density dependence of the mean free path of a nondegenerate neutrino with energy  $E = 1$  MeV in cold neutron matter.<sup>64</sup> Landau theory results obtained including (not including) tensor terms are represented by the solid line (open circles). For comparison, Fermi gas results are also shown, by the dot-dashed line. The dashed line refers to the NMFP obtained without accounting for the collective mode in the spin-density channel.

$|n_{A-1}, \mathbf{p}_n\rangle$  is an eigenstates of the nuclear hamiltonian of Eq.(4), describing the recoiling  $(A - 1)$ -nucleon system with momentum  $\mathbf{p}_n$ .

The use of Eq. (35) allows to rewrite the nuclear transition matrix element in a most simple and transparent form, consisting of the matrix element of the one-nucleon currents between free nucleon states—which can be computed exactly, retaining the fully relativistic expressions of the currents—and the nuclear amplitude involving the target ground state and the state of the recoiling spectator system—which can be safely obtained from non relativistic many-body theory, since no nucleons carrying large momenta,  $\sim \mathbf{q}$ , are involved.<sup>50</sup>

The resulting expression of the differential nuclear cross section is<sup>66</sup>

$$d\sigma_{IA} = \sum_i \int d^3k dE P_i(\mathbf{k}, E) d\sigma_i, \quad (36)$$

where  $d\sigma_i$  is the corresponding cross section describing scattering on the  $i$ -th nucleon, the momentum and removal energy of which are distributed according to the spectral function  $P_i(\mathbf{k}, E)$ .

Accurate theoretical calculations of the nuclear spectral function have been carried out for the few nucleon systems, with  $A \leq 4$ , as well as for isospin symmetric nuclear matter (see Ref. 66 and references therein). For intermediate mass nuclei, realistic spectral functions have been constructed within the Local Density Approximation (LDA), in which the results of nuclear matter calculations are combined with the empirical information extracted from the measured  $(e, e'p)$  cross sections.<sup>67</sup>

It is very important to realise that, owing to the presence of strong nucleon-

nucleon correlations in the nuclear ground state, the recoiling ( $A-1$ )-nucleon system is not necessarily left in a bound, one hole, state. Two hole-one particle states, in which one of the spectator nucleons is excited to the continuum, typically contribute 15-20% of the spectral function normalisation, the corresponding strength being located at large momentum ( $|\mathbf{k}| > 300$  MeV) and energy ( $E > 40$  MeV), well outside the region corresponding to shell model states.

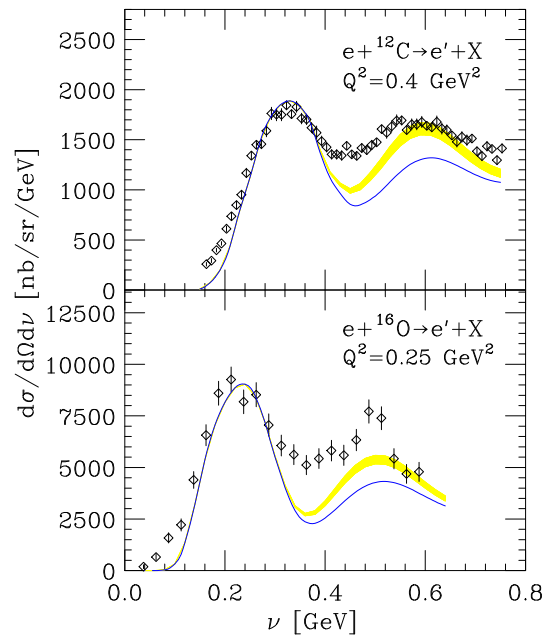


Fig. 7. Top: inclusive electron scattering cross section off carbon at beam energy  $E_e = 1.3$  GeV and electron scattering angle  $\theta_e = 37.5$  deg, corresponding to  $Q^2 = 0.4$  GeV<sup>2</sup> at the  $\Delta$  production peak, as a function of the electron energy loss  $\nu$ . The solid line corresponds to theoretical calculations carried out using the proton and neutron structure functions of Ref. 68, while the shaded region has been obtained with those resulting from the analysis of Ref. 69. The data are taken from Ref. 70. Lower panel: same as in the upper panel, but for oxygen target,  $E_e = 1.2$  GeV and  $\theta_e = 32$  deg, corresponding to  $Q^2 = 0.26$  GeV<sup>2</sup> at the  $\Delta$  production peak. The data are taken from Refs. 71, 72.

### 5.1. Spectral function formalism

To the extent to which the target spectral function is available, Eq. (36) can be used to perform theoretical calculations of the nuclear cross section within the IA. The other required input, i.e. the nucleon cross section  $d\sigma_i$ , can be obtained—at least in principle—from hydrogen and deuteron data. This procedure has been widely employed to analyse the large body of inclusive electron scattering data, both in the quasi elastic sector and beyond pion production threshold. As an example,

Figs. 7 and 8 show the inclusive cross section corresponding to different targets and kinematical setups.

Inspection of Figs. 7 and 8 indicates that the approach based on the IA and the spectral function formalism provides a good description of the data in the quasi elastic sector, corresponding to  $\omega \approx \omega_{QE}$ , in which the elementary electron-nucleon cross section can be written in terms of the proton and neutron vector form factors. On the other hand, the results of Fig. 7 suggest that the available parametrisations of the nucleon structure functions in the region in which the excitation of the  $\Delta$  resonance is the dominant reaction mechanism involve a significant degree of uncertainty. At larger momentum transfer deep inelastic scattering clearly appears to take over at  $\omega \gtrsim \omega_{QE}$ , and the agreement between theory and data over the whole range of energy loss turns out to be remarkably good.

## 5.2. Corrections to the impulse approximation

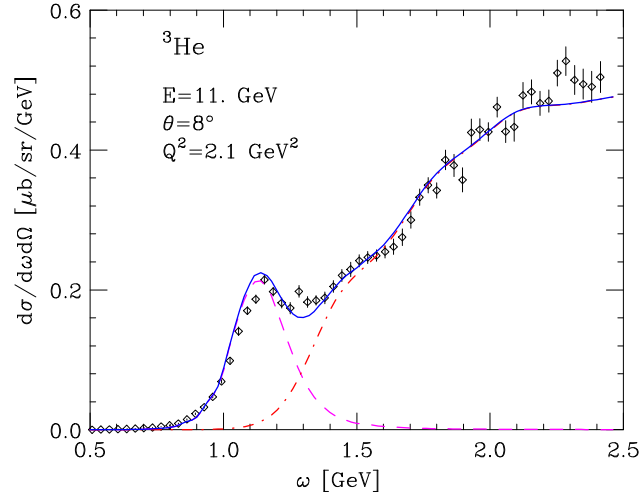


Fig. 8. Inclusive electron scattering cross section off  ${}^3\text{He}$  at beam energy  $E_e = 11$  GeV and electron scattering angle  $\theta_e = 8$  deg, corresponding to  $Q^2 = 2.1$  GeV $^2$  at the quasi elastic peak, as a function of the electron energy loss  $\omega$ . The solid line shows the full theoretical result, while the dashed and dot-dashed lines correspond to the quasi elastic and inelastic contributions, respectively. The data are taken from Ref. 73 (Adapted from Ref. 74).

The capability of obtaining accurate estimates of the nuclear cross section in the quasi elastic channel over a broad kinematical range is important for the interpretation of the signals detected by many neutrino experiments. For example, quasi elastic scattering provides the dominant contribution to the event sample collected by the MiniBooNE Collaboration using a neutrino flux of mean energy  $\sim 800$  MeV.<sup>75</sup>

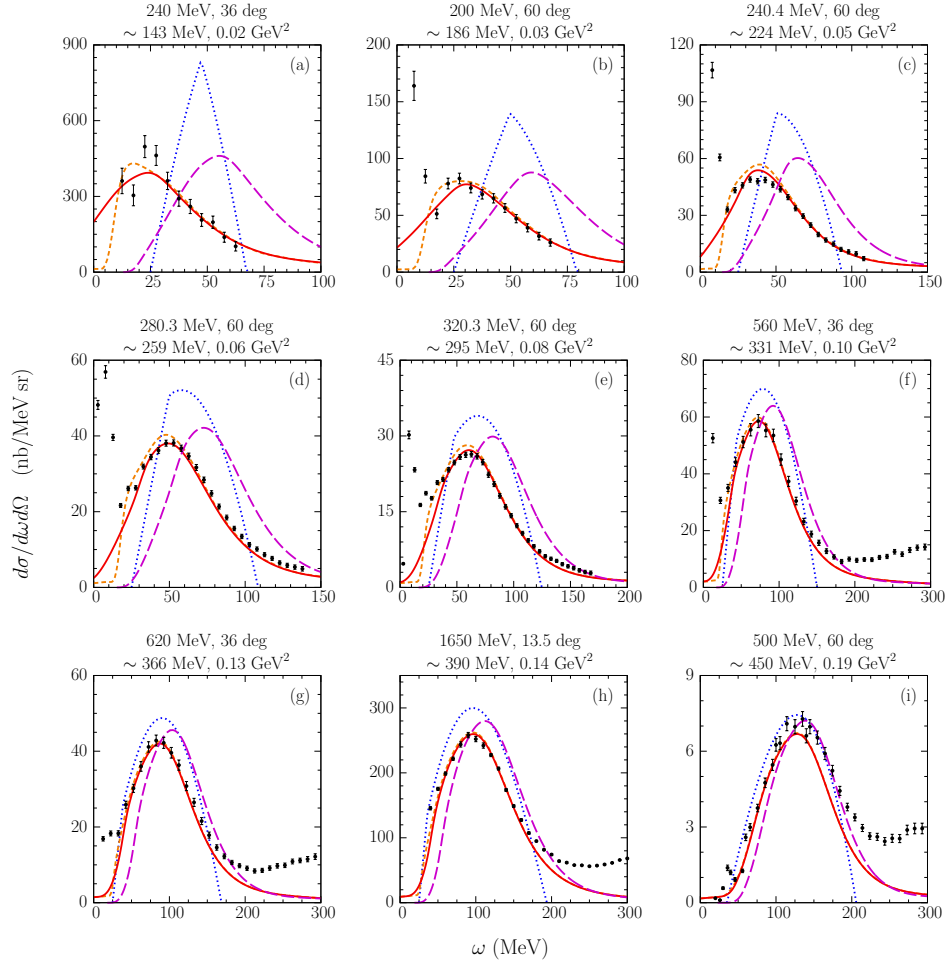


Fig. 9. (color online). Double differential electron-carbon cross sections in the QE channel of Ref. 76, compared to the data of Ref. 78, 79, 80. The solid lines correspond to the result of the full calculation, whereas the long-dashed lines have been obtained neglecting FSI. The difference between the solid and short-dashed lines illustrates the effect of using alternative treatments of Pauli blocking. For comparison, the predictions of the Fermi gas model are also shown, by the dotted lines. The panels are labeled according to beam energy, scattering angle, and values of  $|\mathbf{q}|$  and  $Q^2$  at the quasielastic peak.

The comparison between the results of Ref. 76 and the measured electron scattering cross sections (see Figure 9), suggests that a remarkably good agreement between theory and data in the region of the quasi elastic peak can be achieved correcting the IA results to take into account final state interactions (FSI) between the struck nucleon and the spectators, the effects of which can be described within a generalisation of the spectral function approach, discussed in Ref. 77.

Additional corrections to the IA scheme arise from processes involving two-nucleon currents. It has been suggested<sup>42,81</sup> that the inclusion of these processes, which have been shown to play an important role in the non relativistic regime (see the discussion of Section 4.1.2) may in fact explain the large disagreement between the results of Monte Carlo simulations and the double differential neutrino-carbon cross section measured by the MiniBooNE Collaboration.<sup>75</sup> The generalisation of the factorisation *ansatz* proposed in Ref. 82, 40 will provide a consistent framework to carry out calculations of nuclear amplitudes involving two-nucleon currents, combining the fully relativistic expression of the currents and a description of nuclear dynamics taking into account short range correlations.

## 6. Summary and perspectives

The results of extensive studies carried out over the past decade provide convincing evidence that the model of nuclear structure and dynamics based on non relativistic many-body theory can be exploited to achieve a consistent description of neutrino interactions with nuclei—and, more generally, nuclear matter—over an energy range spanning three orders of magnitude. The availability of such a description will be needed to reach the level of accuracy required by the planned experimental searches of CP violation in the leptonic sector, as well as to significantly improve the modelling of neutrino transport involved in large scale simulations of compact star evolution.

The Monte Carlo approach, while being capable to yield nearly exact results, is—at least for the foreseeable future—limited to the quasi elastic sector and the non relativistic regime. Moreover, its extension to nuclei heavier than carbon would require the use of enormous computing resources. On the other hand, approximation schemes based on the same dynamical model, described by a realistic nuclear hamiltonian, provide a viable alternative approach, suitable for treating the regime of high momentum and energy transfer, in which relativistic effects are important and the hadronic final states involve hadrons other than protons and neutrons.

The picture emerging from the available results suggests that Monte Carlo techniques may be effectively combined with more approximated approaches, to both improve their accuracy and widen their scope. As an example, Monte Carlo estimates—even at variational level—of the nuclear amplitudes involved in spectral function calculations may provide valuable information, useful to reduce the theoretical uncertainty associated with the use of the local density approximation. In addition, the equation of state of cold nucleon matter computed using the Monte Carlo approach will provide more precise benchmarks for the determination of the effective interactions within the formalism of correlated basis function.

The development of a unified description of neutrino interactions based on a realistic model of nuclear interactions—strongly constrained by phenomenology—appears to be possible, and well on its way.

## Acknowledgements

The content of this short review is partly based on a talk given by OB at the Los Alamos National Laboratory, the hospitality of which is gratefully acknowledged. This research is supported by the U.S. Department of Energy, Office of Science, Office of Nuclear Physics, under contract DE-AC02-06CH11357 (AL). The authors are deeply indebted to Artur Ankowski, Joe Carlson, Camillo Mariani, Davide Meloni, Steven Pieper, Noemi Rocco, Makoto Sakuda, Rocco Schiavilla, and Robert Wiringa for countless illuminating discussions on issues related to the subject of this work.

## References

1. O. Benhar, *Int. J. Mod. Phys. E* **58** (2014) 013009.
2. S. Reddy, M. Prakash and J. M. Lattimer, *Phys. Rev. D* **23** (1998) 1430005.
3. J. A. Pons, S. Reddy, J. M. Lattimer and J. A. Miralles, *ApJ* **513** (1999) 780.
4. O. Benhar, N. Farina, H. Nakamura, M. Sakuda and R. Seki, *Phys. Rev. D* **72** (2005) 053005.
5. A. Lovato, C. Losa and O. Benhar, *Nuclear Physics A* **901** (2013) 22 .
6. A. Lovato, O. Benhar, S. Gandolfi and C. Losa, *Phys. Rev. C* **89** (2014) 025804.
7. O. Benhar and G. Veneziano, *Phys. Lett. B* **702** (2011) 433.
8. O. Benhar and D. Meloni, *Nucl.Phys.* **A789** (2007) 379.
9. J. Carlson and R. Schiavilla, *Rev. Mod. Phys.* **70** (1998) 743.
10. A. Lovato *et al.*, *Phys. Rev. Lett.* **111** (Aug 2013) 092501.
11. R. B. Wiringa, V. G. J. Stoks and R. Schiavilla, *Phys. Rev. C* **51** (1995) 38.
12. B. S. Pudliner, V. R. Pandharipande, J. Carlson, S. C. Pieper and R. B. Wiringa, *Phys. Rev. C* **56** (1995) 1720.
13. J. Fujita and H. Miyazawa, *Prog. Theor. Phys.* **17** (1957) 360.
14. M. H. Kalos, *Phys. Rev.* **128** (1962) 1791.
15. R. Grimm and R. Storer, *Journal of Computational Physics* **7** (1971) 134 .
16. D. O. Riska, *Phys. Rep.* **181** (1989) 207.
17. L. E. Marcucci, R. Schiavilla, M. Viviani, A. Kievsky and S. Rosati, *Phys. Rev. Lett.* **84** (2000) 5959.
18. L. E. Marcucci, M. Viviani, R. Schiavilla, A. Kievsky and S. Rosati, *Phys. Rev. C* **72** (2005) 014001.
19. T.-S. Park, D.-P. Min and M. Rho, *Physics Reports* **233** (1993) 341 .
20. T.-S. Park, L. E. Marcucci, R. Schiavilla, M. Viviani, A. Kievsky, S. Rosati, K. Kubodera, D.-P. Min and M. Rho, *Phys. Rev. C* **67** (2003) 055206.
21. S. Pastore, L. Girlanda, R. Schiavilla, M. Viviani and R. B. Wiringa, *Phys. Rev. C* **80** (2009) 034004.
22. M. Piarulli, L. Girlanda, L. E. Marcucci, S. Pastore, R. Schiavilla and M. Viviani, *Phys. Rev. C* **87** (2013) 014006.
23. L. E. Marcucci, R. Schiavilla and M. Viviani, *Phys. Rev. Lett.* **110** (2013) 192503.
24. M. Pervin, S. C. Pieper and R. B. Wiringa, *Phys. Rev. C* **76** (2007) 064319.
25. L. E. Marcucci, M. Pervin, S. C. Pieper, R. Schiavilla and R. B. Wiringa, *Phys. Rev. C* **78** (2008) 065501.
26. R. Schiavilla and R. B. Wiringa, *Phys. Rev. C* **65** (2002) 054302.
27. L. E. Marcucci, M. Piarulli, M. Viviani, L. Girlanda, A. Kievsky, S. Rosati and R. Schiavilla, *Phys. Rev. C* **83** (2011) 014002.
28. R. B. Wiringa and R. Schiavilla, *Phys. Rev. Lett.* **81** (1998) 4317.

24 *Authors' Names*

29. L. E. Marcucci, D. O. Riska and R. Schiavilla, *Phys. Rev. C* **58** (1998) 3069.
30. M. Viviani, R. Schiavilla, B. Kubis, R. Lewis, L. Girlanda, A. Kievsky, L. E. Marcucci and S. Rosati, *Phys. Rev. Lett.* **99** (2007) 112002.
31. J. Lomnitz-Adler, V. Pandharipande and R. Smith, *Nuclear Physics A* **361** (1981) 399 .
32. J. Carlson, S. Gandolfi, F. Pederiva, S. C. Pieper, R. Schiavilla *et al.* (2014) [arXiv:1412.3081 \[nucl-th\]](#).
33. R. B. Wiringa, *Phys. Rev. C* **43** (1991) 1585.
34. J. Carlson, *Phys. Rev. C* **36** (1987) 2026.
35. S. C. Pieper, Quantum Monte Carlo Calculations of Light Nuclei, in *Proceedings of the "Enrico Fermi" Summer School, Course CLXIX, Nuclear Structure far from Stability: New Physics and new Technology*, eds. A. Covello, F. Iachello, R. A. Ricci and G. Maino (IOS Press, Amsterdam, 2008) p. 111. Reprinted in *La Rivista del Nuovo Cimento*, **31**, 709, (2008).
36. K. Schmidt and S. Fantoni, *Physics Letters B* **446** (1999) 99 .
37. S. Gandolfi, A. Lovato, J. Carlson and K. E. Schmidt, *Phys. Rev. C* **90** (2014) 061306.
38. J. Jourdan, *Nuclear Physics A* **603** (1996) 117.
39. A. Lovato, S. Gandolfi, R. Butler, J. Carlson, E. Lusk, S. C. Pieper and R. Schiavilla, *Phys. Rev. Lett.* **111** (2013) 092501.
40. O. Benhar, A. Lovato and N. Rocco (2013) [arXiv:1312.1210 \[nucl-th\]](#).
41. M. Martini, M. Ericson, G. Chanfray and J. Marteau, *Phys. Rev. C* **80** (2009) 065501.
42. M. Martini, M. Ericson, G. Chanfray and J. Marteau, *Phys. Rev. C* **81** (2010) 045502.
43. J. Nieves, I. Simo and M. Vacas, *Phys. Rev. C* **83** (2011) 045501.
44. J. Amaro, M. Barbaro, J. Caballero, T. Donnelly and C. Williamson, *Physics Letters B* **696** (2011) 151 .
45. J. Carlson, J. Jourdan, R. Schiavilla and I. Sick, *Phys. Rev. C* **65** (2002) 024002.
46. A. Lovato, S. Gandolfi, J. Carlson, S. C. Pieper and R. Schiavilla, *Phys. Rev. Lett.* **112** (2014) 182502.
47. A. Lovato, S. Gandolfi, J. Carlson, S. C. Pieper and R. Schiavilla (2015) [arXiv:1501.01981 \[nucl-th\]](#).
48. G. Shen, L. Marcucci, J. Carlson, S. Gandolfi and R. Schiavilla, *Phys. Rev. C* **86** (2012) 035503.
49. LBNE Collaboration, C. Adams, D. Adams, T. Akiri, T. Alion, K. Anderson, C. Andreopoulos, M. Andrews, I. Anghel, J. C. Costa dos Anjos and et al., *ArXiv e-prints* (2013) [arXiv:1307.7335 \[hep-ex\]](#).
50. O. Benhar, A. Lovato and N. Rocco (2015) [arXiv:1502.00887 \[nucl-th\]](#).
51. F. Arias de Saavedra, C. Bisconti, G. Cò and A. Fabrocini, *Phys. Rep.* **450** (2007) 1.
52. A. Akmal and V. R. Pandharipande, *Phys. Rev. C* **56** (1997) 2261.
53. A. Fabrocini and S. Fantoni, in *First International Course of Condensed Matter Physics*, eds. D. Prospero, S. Rosati and G. Violini (World Scientific, Singapore, 1986), p. 87.
54. J. W. Clark, *Prog. Part. Nucl. Phys.* **2** (1979) 89.
55. S. Fantoni and V. R. Pandharipande, *Phys. Rev. C* **37** (1988) 1697.
56. V. R. Pandharipande and R. B. Wiringa, *Rev. Mod. Phys.* **51** (1979) 821.
57. S. Cowell and V. R. Pandharipande, *Phys. Rev. C* **70** (2004) 035801.
58. I. Lagaris and V. Pandharipande, *Nuclear Physics A* **359** (1981) 349 .
59. O. Benhar and M. Valli, *Phys. Rev. Lett.* **99** (2007) 232501.
60. O. Benhar and N. Farina, *Physics Letters B* **680** (2009) 305 .
61. N. Itoh, H. Hayashi, A. Nishikawa and Y. Kohyama, *The Astrophysical Journal Supplement Series* **102** (1996) 411.

62. N. Iwamoto and C. J. Pethick, *Phys. Rev. D* **25** (1982) 313.
63. S. Reddy, M. Prakash, J. M. Lattimer and J. A. Pons, *Phys. Rev. C* **59** (1999) 2888.
64. O. Benhar, A. Lovato and N. Rocco (2013) [arXiv:1312.1210 \[nucl-th\]](#).
65. O. Benhar, A. Cipollone and A. Loreti, *Phys. Rev. C* **87** (2013) 014601.
66. O. Benhar, D. Day and I. Sick, *Rev. Mod. Phys.* **80** (2008) 189.
67. O. Benhar, A. Fabrocini, S. Fantoni and I. Sick, *Nuclear Physics A* **579** (1994) 493 .
68. A. Bodek and J. L. Ritchie, *Phys. Rev. D* **23** (1981) 1070.
69. O. Benhar and D. Meloni, *Phys. Rev. Lett.* **97** (2006) 192301.
70. R. M. Sealock *et al.*, *Phys. Rev. Lett.* **62** (Mar 1989) 1350.
71. M. Anghinolfi *et al.*, *Journal of Physics G: Nuclear and Particle Physics* **21** (1995) L9.
72. M. Anghinolfi *et al.*, *Nucl.Phys.* **A602** (1996) 405.
73. D. Day *et al.*, *Phys. Rev. Lett.* **43** (1979) 1143.
74. O. Benhar and V. R. Pandharipande, *Phys. Rev. C* **47** (1993) 2218.
75. MiniBooNE Collaboration Collaboration (A. Aguilar-Arevalo *et al.*), *Phys.Rev.* **D81** (2010) 092005.
76. A. M. Ankowski, O. Benhar and M. Sakuda, *Phys. Rev. D* **91** (2015) 033005.
77. O. Benhar, *Phys. Rev. C* **87** (2013) 024606.
78. P. Barreau *et al.*, *Nucl. Phys. A* **402** (1983) 515.
79. D. T. Baran *et al.*, *Phys. Rev. Lett.* **61** (1988) 400.
80. R. R. Whitney, I. Sick, J. R. Ficenec, R. D. Kephart and W. P. Trower, *Phys. Rev. C* **9** (1974) 2230.
81. J. Nieves, I. Ruiz Simo and M. Vicente Vacas, *Phys.Lett.* **B707** (2012) 72.
82. O. Benhar and N. Rocco (2013) [arXiv:1310.3869 \[nucl-th\]](#).